J Mater Sci (2010) 45:2042–2050
DOI 10.1007/s10853-009-4135-y

HTC2009

Interaction between liquid aluminum and yttria substrate: microstructure characterization and thermodynamic considerations

J. Wojewoda-Budka · N. Sobczak · B. Onderka · J. Morgiel · R. Nowak

Received: 12 June 2009 / Accepted: 16 December 2009 / Published online: 5 January 2010

Abstract The systematic microstructure and thermodynamic studies of the reactions between liquid aluminum and dense polycrystalline yttria (Y_2O_3) substrates at 1,273 K are reported in this article. The microstructure observations showed the presence of three reaction product zones extending ~1 mm into the oxide substrate of typical C4 (Co-Continuous-Ceramic-Composites) structure. The first zone starting from the drop side was composed of fine crystalline precipitates of the $Al_5Y_3O_{12}$ (YAG) phase dispersed in the Al_3Y matrix. The second zone was built of larger $AlYO_3$ (YAP) crystals. The third zone formed elongated oxide precipitates (YAP) surrounded by the Al_2Y intermetallic channels. The thermodynamic calculation indicated that, depending on the amount of the yttrium dissolved in aluminum, the YAG (up to 5 at.% Y), YAP (5–13 at.% Y), or Al_2Y for higher content of yttrium might form at 1,273 K, while the Al_3Y phase might appear during cooling.

Introduction

Metal–ceramic Al–Al_2O_3 composites can be produced in situ by the reaction between the liquid aluminum and metal oxides like NiO, CoO, SiO_2, ZnO, mullite, or kaolinite. Due to the oxy-redox reactions schematically expressed in Eqs. 1 and 2, a characteristic microstructure appears in the form of continuous and mutually interpenetrating ceramic and metallic phase lattices.

$$2\mathrm{Al} + 3/y\mathrm{MeO}_x \rightarrow x\mathrm{Al}_2\mathrm{O}_3 + 3/y\mathrm{Me} \quad (1)$$

$$(x+2)\mathrm{Al} + 3/y\mathrm{MeO}_y \rightarrow \mathrm{Al}_2\mathrm{O}_3 + \mathrm{Al}_x\mathrm{Me}_{3/y} \quad (2)$$

Such a morphology is called C4 type structure (Co-Continuous-Ceramic Composites) [1–3] and it involves the unique features like high modulus, high strength, and resistance to the thermal shocks. The C4 features and their in situ production open the possibility for the application of such light and inexpensive metal–ceramic materials in the car industry. They can also be applied in the vehicles used in mining.

The type and morphology of reactively formed products can vary, depending on a starting reactive oxide [4]. For example, the reaction product region (RPR) of TiO_2 and ZrO_2 can be described as separate Al_2O_3 crystals formed at the Al/oxide interface. Such a layer tends to be very thin. On the contrary, the oxides like ZnO, SiO_2, $B_{13}O_2$, mullite, kaolin react with aluminum and form the thick RPR of C4, in which the Al_2O_3 network and metallic Al(Me), Me, or $Al_xMe_{3/y}$ network interpenetrate each other. The RPR is located inside the substrate and the alumina size can be from nanometers up to few tens of micrometers. These differences are attributed to two factors: volumetric mismatch between the initial oxide and Al_2O_3 and the solubility of the freshly formed Me product in the aluminum. In the first case, both factors are negligible, while in the second one, the volumetric mismatch leads to high tensile stresses in the Al_2O_3 phase, which together with high solubility of metal Me in Al contributes to the formation of

J. Wojewoda-Budka (✉) · J. Morgiel
Institute of Metallurgy and Materials Science, Polish Academy of Sciences, 25, Reymonta St., 30-059 Cracow, Poland
e-mail: nmwojewo@imim-pan.krakow.pl

N. Sobczak · R. Nowak
Foundry Research Institute, 73, Zakopianska St., 30-418 Cracow, Poland

B. Onderka
Faculty of Non-Ferrous Metals, AGH University of Science and Technology, 30, Mickiewicza Ave., 30-059 Cracow, Poland

discontinuities in the Al_2O_3 layer, followed by the reactive metal impregnation, where the C4 structure is obtained as a final stage.

Another mechanism operates for the cobalt and nickel oxides. Here, the nanoscale precipitates form a broad and layered microstructure inside the drop and the substrate. At the beginning, the discontinuous Al_2O_3 layer forms due to the interaction of the oxide and Al, for which the volumetric mismatch MeO–Al_2O_3 is significant. Next, the metal (Ni or Co) reacts with the molten Al creating the intermetallic phases (Al_3Ni, Al_9Co_2, and $Al_{13}Co_4$) inside the metal channels. The RPR, composed of alumina and intermetallics, cracks and separates from the substrate due to the already mentioned volumetric mismatch and resulting stresses. These two stages are periodically repeated and finally layered structure is formed.

Recently, Barzilai et al. [5, 6] have reported that during heating at 1,423 K, the liquid aluminum reduces yttria (Y_2O_3) to form a thick reaction products region. This allows considering the Al–Y_2O_3 system as a potential candidate for in situ composite synthesis. The study performed by Barzilai et al. showed that due to the Al–Y_2O_3 reaction, the $AlYO_3$ phase was formed inside the RPR. Later, a clear evidence for the creation of the C4 structure was derived by Sobczak et al. [7] for the temperature range of 1,073–1,273 K.

The results presented in this work are the part of the project concerning the interaction of the aluminum and Y_2O_3 substrate. The studies have been stimulated by the fact that Al-containing melts have high-temperature contact with the Y_2O_3-containing refractory ceramics, widely used in the production of crucibles and various foundry appliances. The RPR formed due to the contact heating at 1,273 K reveal complex morphology. No alumina was found to be inside the RPR. Instead of that the ceramic phase network was composed mainly of the yttrium aluminum perovskite (YAP–$AlYO_3$) and also yttrium aluminum garnet (YAG–$Al_5Y_3O_{12}$), while the Al_2Y or Al_3Y represented the metallic phase.

The microstructure aspects are supplemented by the thermodynamic considerations. The assessment given by Fabrichnaya et al. [8] allowed calculating the isothermal cross-section of the Al–Y–O phase diagram. It was also possible to calculate and compare the reaction constant of the YAP formation with the literature data [5].

Experimental

The Al/Y_2O_3 couples were produced from pure Al (99.9999%) and the Y_2O_3 polycrystalline ceramic substrate in the sessile drop wettability test as described in [9]. The Y_2O_3 substrates were produced by high-pressure synthesis and polished up to 120 nm roughness. Directly before the wettability test, all surfaces of aluminum were mechanically cleaned.

Then, both Al and Y_2O_3 specimens were ultrasonically cleaned in acetone and placed in a vacuum chamber. In the sessile drop wettability tests, the contact heating up to 1,273 K at the rate of $\sim$10 K/min and then at 1,273 K for 120 min in a dynamic vacuum was applied. After testing, the Al/Y_2O_3 couples were cooled down at the rate of $\sim$10 K/min. For the analysis of the microstructure and chemical composition of the reactively formed products, the couples were cross-sectioned perpendicularly to the substrate surface, grinded and polished with a diamond suspension up to 1 μm. Special attention was paid to obtain accurate parallel surfaces of the specimens. The microstructure was examined by the optical microscope (Inspection Zoom Microscope EQ-MS-ZMKZ∅3, MTI). Next, the samples were investigated with the Philips XL 30 and FEI E-SEM XL30 Scanning Electron Microscopes (SEM) equipped with the Link ISIS, EDAX X-ray energy dispersive spectrometers (EDS), respectively. The selected areas of the RPR were cut using the Quanta 3D Focused Ion Beam (FIB) in order to prepare thin foils for the transmission electron microscopy (TEM) observations. The TEM investigations were performed using TECNAI G^2 FEG super TWIN (200 kV) microscope equipped with High Angle Angular Dark Field (HAADF) detector integrated with the EDAX energy dispersive X-ray spectroscopy system.

The X-ray diffraction measurements were performed using the filtered CuKα radiation by means of Bruker D-8 Discover diffractometer. X-ray tube radiation was focused using polycapillar optics ensuring a near-parallel incident beam. The beam size was approx. 1 mm in diameter. Experimental data were analyzed using EVA software with ICDD PDF-2 database.

Results and discussion

Microstructure and phase composition

The observations of the cross-sectioned Al/Y_2O_3 couple showed the existence of large precipitates of intermetallic phase inside the initially pure Al drop and an irregular wavy shape of the obtained RPR in the oxide substrate (Fig. 1). The intermetallic precipitates were present inside the whole drop, while the RPR revealed a characteristic shape, where the region corresponding to the central part of the droplet was thinner compared with its periphery. Such morphology differed from that reported by Sobczak [4] for other Al/MeO couples. Moreover, the Al/Y_2O_3 couples produced by Barzilai et al. [5, 6] after the interaction at

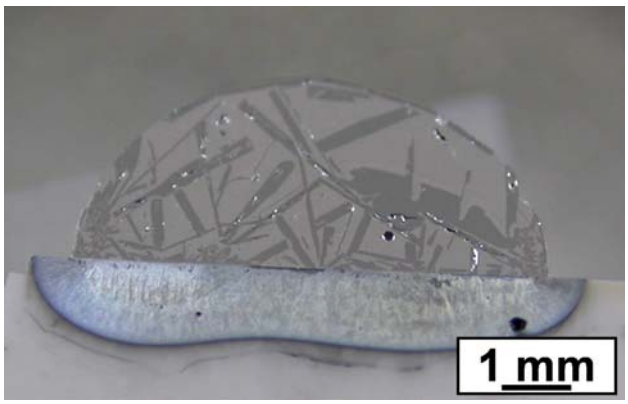

Fig. 1 The microstructure of the cross-sectioned Al/Y_2O_3 couple after contact heating at 1,273 K for 2 h

higher temperature of 1,423 K did not show anything like that. Such a rather unusual shape of RPR could result from dissimilar conditions of the mass transfer in the central and in the peripheral parts of the Al droplet, as was discussed in details by Sobczak [10] on the example of AlTi6/mullite couples. Recently, more detailed research by Sobczak et al. [11] on factors affecting the shape of RPR in the Al/Y_2O_3 couples has demonstrated an important role of the primary oxide film on the Al specimen by using the Y_2O_3 substrates of different positions (horizontal, vertical) and various roughness (grinded or polished up to 120 nm). A widely accepted opinion is that the native oxide film can be in situ removed from the aluminum droplet in vacuum at $T > 1{,}173$ K mainly due to the formation of gaseous aluminum suboxide Al_2O. However, Sobczak et al. have demonstrated that this process does not take place homogeneously along the drop/substrate contact, i.e., it is more effective in the drop periphery, while, in its central part, it is less pronounced, since the evacuation of gaseous product (Al_2O) might be suppressed, particularly in the case of polished substrates. For the 1,273 K test with polished substrates, the residual native oxide film, preventing a true contact between Al and a substrate during their contact heating, affects the reactivity and thus much thinner RPR is recorded in the central part of the droplet. On the contrary, under the same testing conditions, the RPR of uniform thickness was observed with grinded vertical Y_2O_3 plate because in the case of rough substrate surface, numerous discontinuities in the drop/substrate contact play a role of open channels for free evacuation of gaseous product resulting in more effective removal of interfacial oxide and thus creating comparable conditions in the center and the periphery of the drop [11]. This explanation is in agreement also with the results obtained for the Al/Y_2O_3 couple by Barzilai et al. [5, 6] because in their case much higher temperature of 1,423 K created similar conditions in spite of different mechanism, i.e., the dissolution of oxide film in liquid aluminum was a major factor responsible for the oxide removal at high temperature and it took place uniformly along the whole drop/substrate contact.

A closer inspection using the SEM revealed that the RPR was composed of the three zones (RPZ) of different thickness, structure, and chemistry (Fig. 2). The first RPZ of up to 100 μm of thickness was located just next to the drop (Fig. 2a, b), the second one was very narrow (up to 25 μm) and composed of large crystals (Fig. 2a, c) while

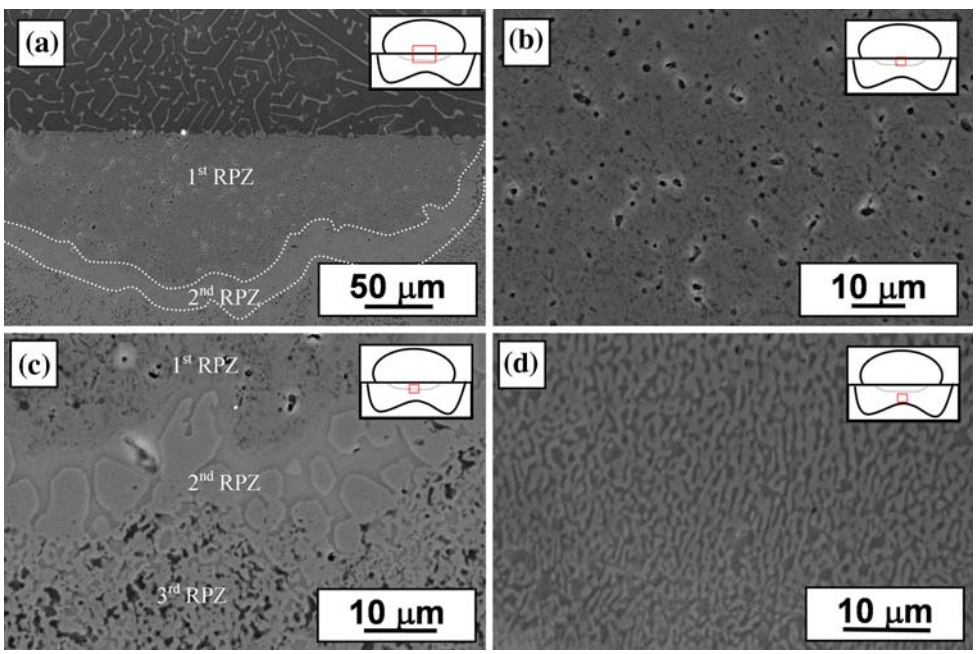

Fig. 2 SEM micrograph of the Al/Y_2O_3 couple after contact heating at 1,273 K. Three reaction product region zones can be distinguished: first next to the drop, second marked with *dotted lines* in **a** and third next to the Y_2O_3 substrate. The interface Al/first RPZ/second RPZ is presented in **a**. The microstructures of the first, second, and third reaction product zones are presented in **b**, **c** and **d**, respectively. *Boxes* inserted in the right corner of figures show the places, where microstructure images were taken

the third RPZ, located next to the substrate, was the widest (Fig. 2c, d).

The EDS analysis performed across the RPR showed that the first RPZ contained 40 at.% Al, 18 at.% Y, and 48 at.% O. The next layer was enriched in aluminum (70 at.%) and yttrium (close to 30 at.%) with simultaneous drastic decrease in the oxygen amount (up to negligible level) and it was found to correspond relatively thick metallic channels surrounding the large crystals in the second RPZ. The values for the largest area, described as third RPZ, varied from 25–65 at.% for Al to 8–55 at.% for O.

The typical X-ray diffraction pattern obtained for the Al/Y_2O_3 couple is shown in Fig. 3. The existence of $Al_5Y_3O_{12}$ (YAG) and $AlYO_3$ (YAP) phases was clearly detected. Moreover, the Al_3Y phase was identified, mainly coming from large crystals in the drop, while the Y_2O_3 signal present in the pattern originated from the substrate. The Al_2Y and $AlYO_3$ patterns were very similar, thus difficult to distinguish from each other.

The application of FIB thin foil preparation technique allowed the TEM examination at precisely defined areas: first/second RPZs and third RPZ/Y_2O_3. Figures 4, 5 show the bright field images of the microstructure taken of both areas together with scanning-transmission mode images which visualize differences in the chemical composition and also show more clearly the interpenetrating channels (Fig. 5a, b).

The TEM microstructure of first/second RPZs interface can be divided into three areas denoted as A, B, and C (Fig. 4a, b). The EDS analysis of corresponding selected area electron diffraction (SAED) patterns [12] showed that

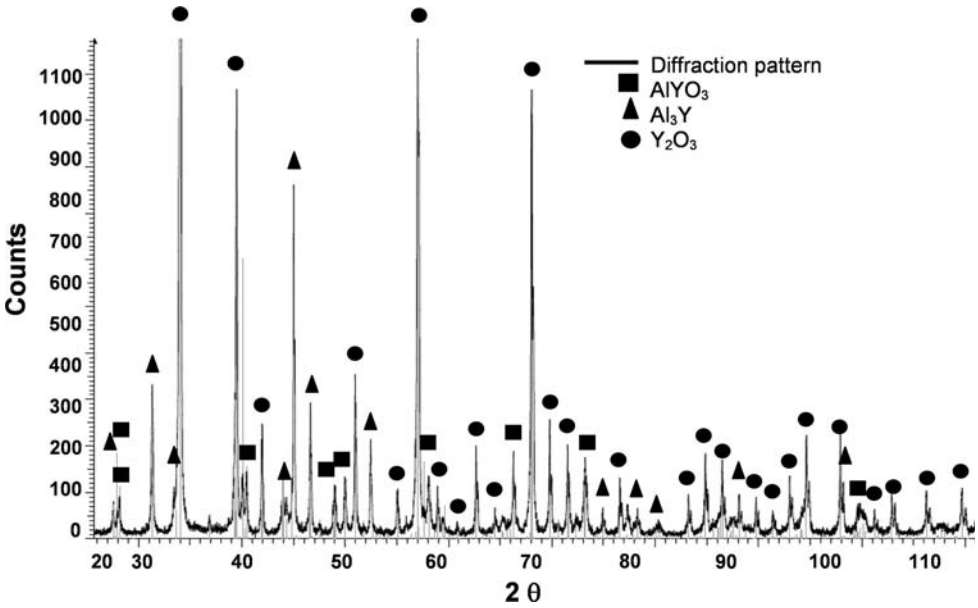

Fig. 3 X-ray diffraction pattern of the Al/Y_2O_3 couple produced at 1,273 K

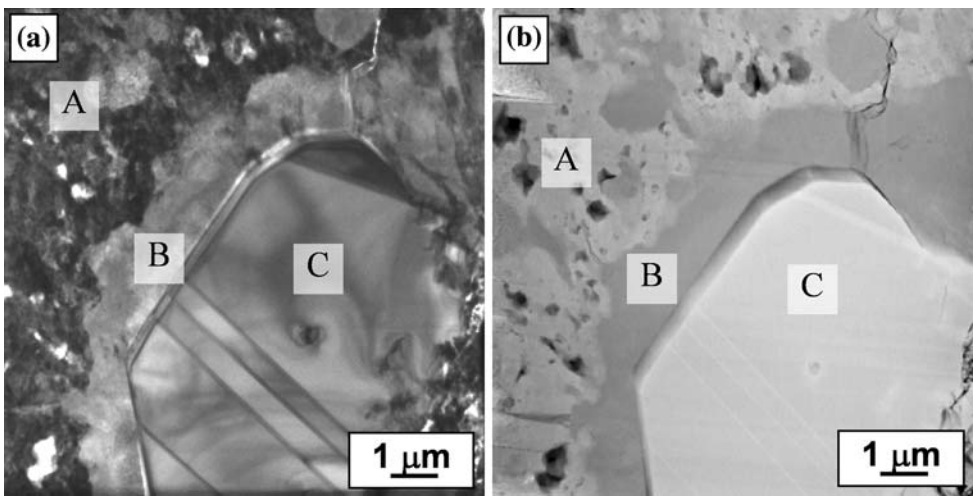

Fig. 4 TEM micrograph of the first RPZ/second RPZ interface (**a**) together with its STEM image (**b**). Three characteristic areas were marked as A, B, and C

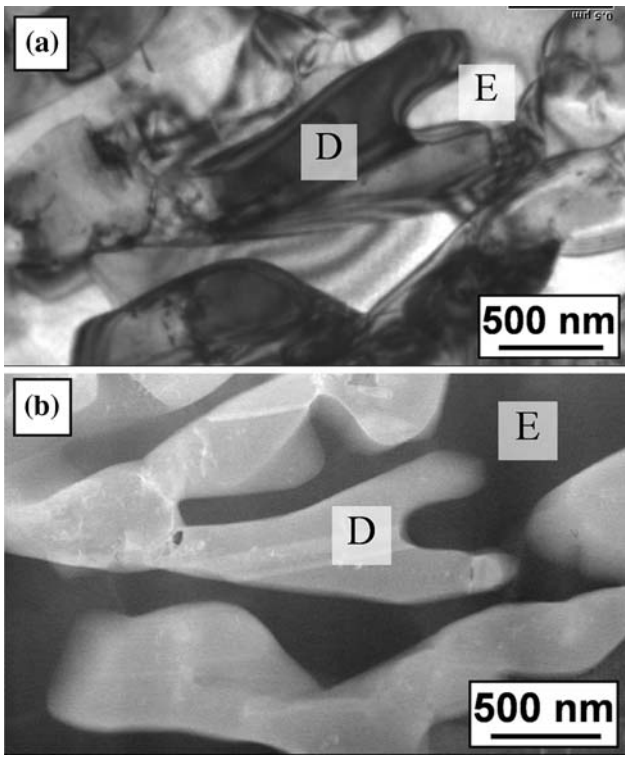

Fig. 5 TEM microstructure of the third RPZ/Y_2O_3 interface (**a**) together with its STEM image (**b**). Ceramic and metallic phases forming interpenetrating channels were marked as D and E, respectively

fine crystalline zone A was probably YAG ($Al_3Y_5O_{12}$) phase, big crystal C consisted of YAP ($AlYO_3$) phase, while interfacial layer B, most probably, corresponded to the Al_3Y phase nucleated from the Y-rich Al(Y) liquid solution at the $AlYO_3$ during cooling. The Al_3Y precipitates intermixed with the $Al_3Y_5O_{12}$ ones were also noted between the $AlYO_3$ crystals. It can be summarized that the A area corresponded to the fine grained first RPZ and the second RPZ was decorated with the crystals like the C one.

The second investigated area located at the substrate–side interface showed typical C4 type microstructure (Fig. 5a, b), where the metallic and ceramic phases form interpenetrating networks. The maps of elements distribution [12] taken from this place revealed that Al, Y, and O were present inside the long precipitates, while inside the matrix, only Al and Y were found. The combination of two complex techniques—EDS analysis and SAED patterns indicated that the precipitates consisted of $AlYO_3$ while the matrix was composed of Al_2Y [12]. However, the size of $AlYO_3$ precipitates was smaller compared with that of the second zone. Such a difference of $AlYO_3$ size depended on their location and it was previously observed in other reactive Al/oxide couples [4]. As explained by Sobczak [4], the phenomenon was caused by different mechanisms of growth of oxide precipitates: fine Al_2O_3 precipitates in the RPR were created inside the reactive substrate due to the redox reaction while the coarse Al_2O_3 precipitates, nucleated at the drop-side interface and always growing into the droplet, were similar to those observed in nonreactive pure Al/Al_2O_3 and Al–Me/Al_2O_3 couples and formed due to dissolution–precipitation mechanism. When redox reaction in Al/oxide couple was accompanied with substrate cracking due to volumetric mismatch, the freshly formed crack was filled with the liquid metal. In such a case the structural transformations at the newly formed additional Al/substrate interface inside the substrate was similar to the primary drop/substrate interface. Thus, the formation of coarse Al_2O_3 precipitates by dissolution–precipitation mechanism was also possible in a wide metallic channel created by the substrate cracking. The explanation was in agreement with the detailed examination of the structure between different regions that evidenced the presence of microcracks between the first and third RPZs and just suggesting that the formation of the second RPZ took place after cracking inside the substrate during high-temperature testing. EDS analysis performed on the scanning electron microscopy of the second RPZ stayed in opposite to the results from the TEM studies. However, SEM–EDS analyses were performed as a line scan across the drop and RPR zone. This line scan probably omitted the big YAP crystal, gathering the data mostly from the surrounding Al_3Y channels and also YAP crystals. The described RPR microstructure is schematically showed in Fig. 6.

Thermodynamic considerations

Knowledge of the temperature–composition (*T*–*x*) phase diagrams and thermochemical properties of the Al–Y–O system can provide guidance in optimizing the Al/Y_2O_3 reaction establishing the thermal processing limits of oxide compounds and alloys. This is true even for nonequilibrium processing routes since the distance from or driving force to the equilibrium state should be discussed quantitatively. For the ceramic layer applications it is important to clarify the stable and the unstable compositions (example Fig. 7) of the oxide materials. Hence, the thermodynamic phase stabilities and the temperature–composition phase diagrams are important for an understanding of the boundary conditions of a variety of processing steps.

The investigations [5, 6] concerning the results of the Al/Y_2O_3 system revealed that Al reacts with Y_2O_3, forming $Al_5Y_3O_{12}$ (YAG) and $AlYO_3$ (YAP) oxide compounds beneath the drop releasing Y, which dissolves in the melt. The experimental data of the present work confirms that a certain amount of Y is transferred into the melt during the reaction of Y_2O_3 with liquid Al.

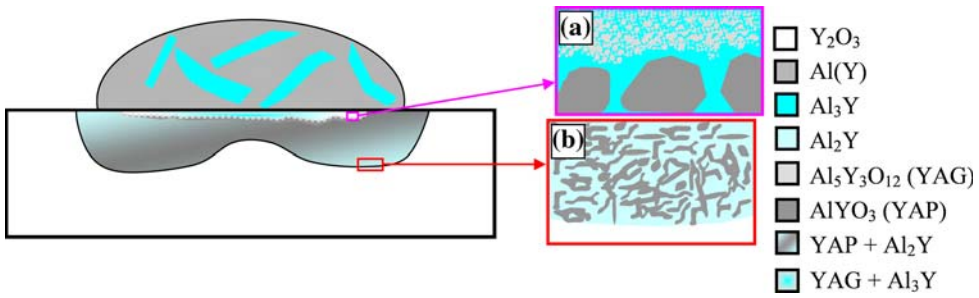

Fig. 6 Scheme of microstructure changes of reaction product region formed in Al/Y_2O_3 couple after contact heating at 1,273 K. Two enlarged *boxes* show interfaces of first RPZ/second RPZ (**a**) and third RPZ/Y_2O_3 (**b**)

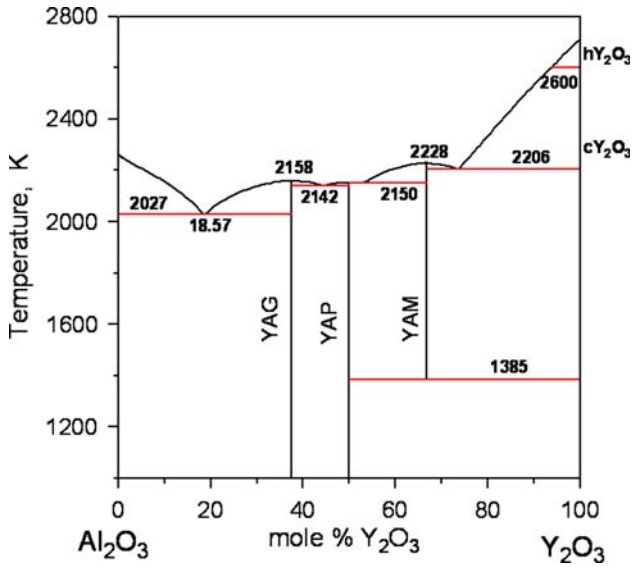

Fig. 7 Calculated pseudobinary phase diagram of Al_2O_3–Y_2O_3. Symbols cY_2O_3 and hY_2O_3 denote yttrium oxide of cubic and hexagonal structures, respectively. Al_2O_3 has a structure of corundum

As it was observed, the reaction is accompanied by the formation of thick RPR at the metal/oxide interface. The chemical interaction that takes place in this system can be expressed by the following possible chemical reactions:

$$1/2Y_2O_3 + \underline{Al} = 1/2Al_2O_3 + \underline{Y} \quad (3)$$

$$4/5Y_2O_3 + \underline{Al} = 1/5Al_5Y_3O_{12} + \underline{Y} \quad (4)$$

$$Y_2O_3 + \underline{Al} = AlYO_3 + \underline{Y} \quad (5)$$

in which underline indicates Al solution and Y dissolved in liquid solution.

The thermodynamic analysis of interface reactions proposed by Barzilai et al. [5] based on the assumption that the amount of the dissolved Y in the Al melt formed the YAP phase. As the standard free Gibbs energy change during all of the proposed reactions (3–5) is >0, such reactions are not spontaneous and after reaching the equilibrium should stop without a shifting factor. Hence, the Y content in the Al-based solution increases until the system reaches the equilibrium conditions. The thickness of the RPR is controlled by the thermodynamic properties of the oxide phases and by the components activity in the melt. The profile of RPR should be controlled by the diffusion path conditions.

The equilibrium constants K_i ($i = 3\ldots5$) of reactions (3–5) are equal to:

$$K_i = \exp\left(\frac{-\Delta G^0_{(i)}}{RT}\right) = \frac{a^{(i)}_Y}{a^{(i)}_{Al}}, \quad (6)$$

where a_Y and a_{Al} are the activities of Y and Al in the melt, respectively.

According to Barzilai et al. [5] analysis, the equilibrium constant K_5, for reaction (5) at 1,423 K is equal to

$$K_5 = \frac{a_{Y(5)}}{a_{Al(5)}} = 6.5 \cdot 10^{-4} \quad (7)$$

This activity ratio (a_Y/a_{Al}) in the binary Al–Y solution was calculated using Redlich–Kister polynomial approach [13] for the reaction (5) predominant at 1,423 K. From that analysis, it can be concluded that the yttrium is dissolved in the melt and the $AlYO_3$ formation takes place when the activity ratio (a_Y/a_{Al}) is $<6.5 \cdot 10^{-4}$.

The validity analysis of Barzilai et al. [5] is unfortunately limited to the YAP precipitation and does not take into consideration the reactions corresponding to the formation of YAG phase as well as intermetallic phases according to the Al–Y binary phase diagram data (Fig. 8). They calculated the activities along the composition path $X_O = 0$ (Fig. 10) and such assumption is valid since the oxygen solubility in Al–Y liquid solution is very low because of the high stabilities of aluminum and yttrium oxides and their compounds in the Al–Y–O system. However, they neglected the solubility limit of Y in the liquid Al beyond which the Al_2Y precipitation (or Al_3Y below 1,253 K) should be observed (Fig. 8). In addition, Barzilai et al. [5] used thermodynamic data from old tables [14] together with the newest assessments and mixed them in one procedure. The calculation carried out in the present work was based on the CALPHAD assessments [15] of Al–Y–O system and shows that such mixed procedure leads to the incompatibilities of equilibrium constants. According to that assessment, the (a_Y/a_{Al}) ratio for the reaction (5) is five times lower (Fig. 9). In the present work, the equilibrium constants K_i ($i = 3\ldots5$) of reactions

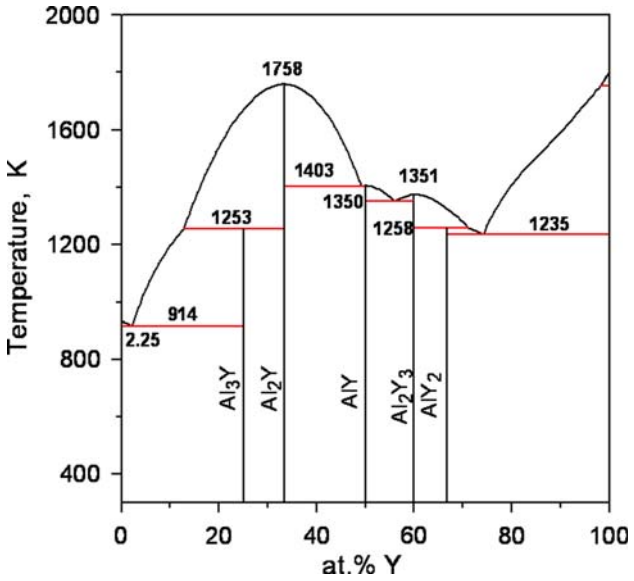

Fig. 8 The Al–Y phase diagram calculated in this work according the model description of Fabrichnaya et al. [8]

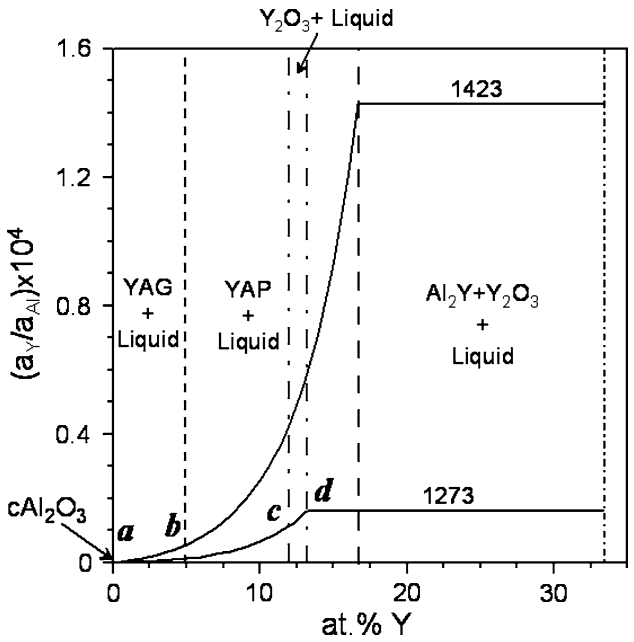

Fig. 9 The comparison of activities ratios of reaction (5) as a function of yttrium concentration in Al–Y liquid solution calculated at 1,273 and 1,423 K. The contact areas of Al-rich liquid with Al_2O_3, YAG, and YAP oxide compounds and $Al_2Y + Y_2O_3$ are indicated

(3–5) were calculated using Fabrichnaya et al. [8] thermodynamic assessment of the phases in the Al–Y–O system. The liquid solution was modeled as an ionic solution [16], in which the neutral $AlO_{1.5}$ species are located in the anion sublattice.

According to the ternary phase diagram calculated at 1,273 K based on the thermodynamic assessment of Al–Y–O system [8], the Al(Y) liquid solution can be in the equilibrium with the Al_2O_3, YAG, YAP or Al_2Y (or $Al_2Y + Y_2O_3$). However, the ratios of activities calculated as a function of yttrium in Al(Y) liquid solution at temperatures 1,273 and 1,423 K [8] show the negligible range of stability of Al_2O_3 in the contact with such melt (Fig. 9). It seems that the influence of continuous pumping (dynamic vacuum conditions) on the oxide formation (Le Chatelier–Braun Principle) is relatively low due to the mentioned stability of all the oxides present in the Al–Y–O system.

The horizontal lines in Fig. 9 represent three phase regions, corresponding to the limit of Y solubility in the liquid Al. This solubility limit cannot be omitted in thermodynamic analysis of reaction of Al with Y_2O_3. The comparison of Barzilai's and present work activity calculation paths is shown in enlarged Al-rich corner of isothermal cross-section of the Al–Y–O phase diagram calculated at 1,273 K (Fig. 10). Barzilai's activity calculation path was determined along $X_O = 0$ composition while our calculation was computed along the liquidus curves.

The Al–Y–O diagram calculated at 1,273 K (Fig. 11) shows the significant ranges of Al–Y liquid solutions in the equilibrium with the YAG and YAP compounds. As long as Y content in the melt is below the equilibrium curve, the Y_2O_3 decomposition with increasing Y concentration in the melt and a sequence of the $Al_5Y_3O_{12}$ and $AlYO_3$ formation is expected.

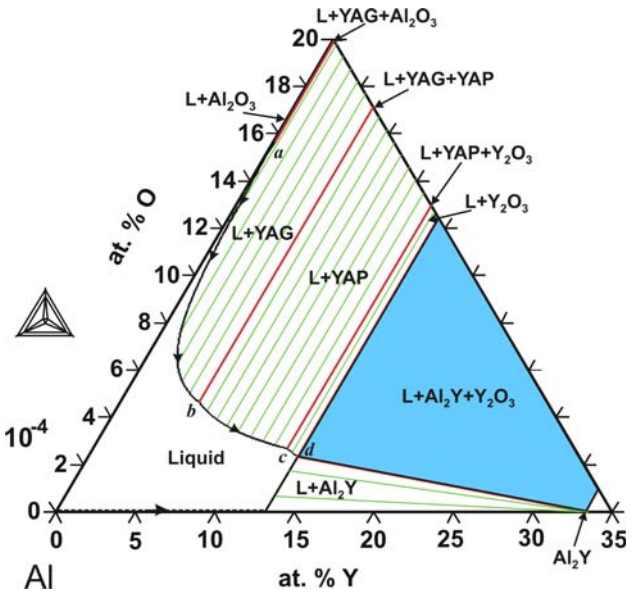

Fig. 10 The enlarged Al-rich corner of isothermal cross-section of Al–Y–O phase diagram calculated at 1,273 K. The *lines* inside the two-phase areas represent tie-lines. The activity calculation paths obtained by Barzilai's [5] and resulting from present studies are indicated by *solid* and *dotted arrows*, respectively

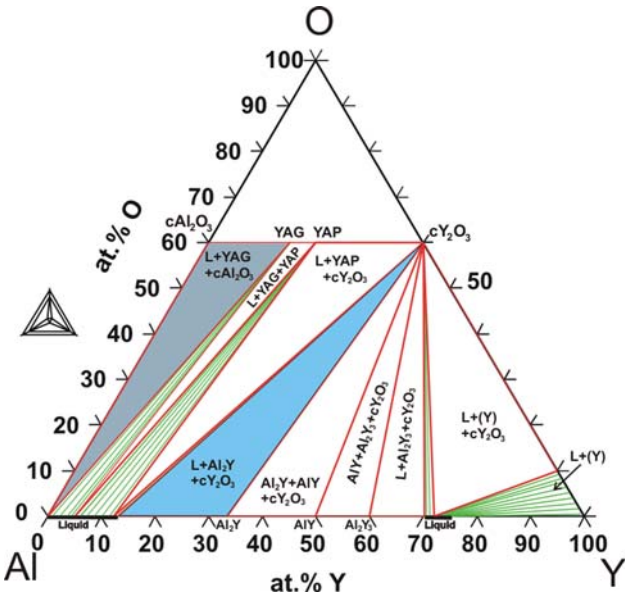

Fig. 11 Isothermal cross-section of Al–Y–O phase diagram calculated at 1,423 K [8]. The *lines* inside the two-phase areas represent tie-lines

The pure Al_2O_3 is in the equilibrium with almost pure aluminum (solubility limit is of the order of 0.16 at.% Y and $1.6 \cdot 10^{-3}$ at.% O) and YAG compound and the formation of one of such compounds depends on the kinetic properties of the system and interface. The formation of mixed oxides layers is directly related with the diffusion rate of components through the interface between liquid Al solution and Y_2O_3 substrate. Such kinetic conditions together with the evolution of diffusion path are responsible for the wavy shape of the RPR in Al/Y_2O_3 couple [17].

One should also consider that some amount of Al_2O_3 phase formed during the reaction at the Al/Y_2O_3 interface can react with Y_2O_3 and/or YAP to form YAG:

$$5Al_2O_3 + 3Y_2O_3 = 2Al_5Y_3O_{12} \quad (8)$$

$$Al_2O_3 + 3AlYO_3 = Al_5Y_3O_{12} \quad (9)$$

The Gibbs energy change of such reaction is negative at 1,273 K apart from the dataset used in calculations [8, 18]. Thus, the reactions (8 or 9) are responsible for the YAG layer formation in the first zone in the substrate under the aluminum droplet.

In this study, the presence of Al_3Y intermetallic compound inside the drop, according to the Al–Y phase diagram (Fig. 8), can be explained by the formation during sample cooling.

Conclusions

The reactivity of liquid aluminum with yttrium oxide substrate at 1,273 K was examined taking into account both the experimental data and thermodynamics of the Al–Y–O system. The microstructure observations showed the presence of three reaction product zones extending ~1 mm into the oxide substrate of typical C4 structure. The first zone starting from the drop side was composed of the fine crystalline precipitates of $Al_5Y_3O_{12}$ (YAG) phase interspersed in the Al_3Y matrix. The second zone was built of larger $AlYO_3$ (YAP) crystals surrounded by the metallic phase. The third zone formed the elongated oxide precipitates (YAP) surrounded by the Al_2Y intermetallic channels.

The ternary Al–Y–O phase diagram was calculated based on the CALPHAD thermodynamic assessment and the isothermal cross-section for 1,273 K was defined. The equilibrium constants of reactions were calculated using Fabrichnaya et al. thermodynamic assessment of phases in the Al–Y–O system and the liquid solution was modeled as an ionic solution in which the neutral $AlO_{1.5}$ species are located in the anion sublattice. The Al–Y–O diagram calculated at 1,273 K showed the significant ranges of Al–Y liquid solutions in the equilibrium with the YAG and YAP compounds. As long as Y content in the melt was below the equilibrium curve, the Y_2O_3 decomposition with increasing Y concentration in the melt and a sequence of the $Al_5Y_3O_{12}$ and $AlYO_3$ formation was expected. Two facts should be taken into account during the YAG formation. The first one is that the pure Al_2O_3 is in the equilibrium with almost pure Al and YAG compound and their formation depends on the kinetic properties of the system and interface. The second fact is that some amount of Al_2O_3 phase formed during the reaction at Al/Y_2O_3 interface can react with Y_2O_3 and/or YAP to form YAG in the reactions: $3AlYO_3 + Al_2O_3 \rightarrow Al_5Y_3O_{12}$ or $5Al_2O_3 + 3Y_2O_3 \rightarrow 2Al_5Y_3O_{12}$. On the other hand, the YAP compound of the interwoven microstructure can be found as a perfect composite material taking into account the transfer of stresses and resistance to crack propagation.

The obtained results demonstrated that the interaction between liquid aluminum and dense polycrystalline Y_2O_3 had a complex character and contrary to other Al/MeO systems (MeO—reactive oxide such as SiO_2, ZnO, CoO, NiO, and mullite) led to the formation of mainly ternary oxides of YAG and YAP types while the metallic network formed was composed of intermetallic Al_2Y and Al_3Y phases.

Acknowledgements This research was performed in the frame of grant for young researchers under the START programme of the Foundation for Polish Science.

References

1. Clarke DR (1992) J Am Ceram Soc 75:739
2. Breslin MC, Ringnalda J, Xu L, Fuler M, Seeger J, Daehn GS, Otani T, Fraser HL (1995) Mater Sci Eng A 195:113

3. Liu W, Koster U (1996) Scr Mater 35:35
4. Sobczak N (2005) Solid State Phenom 101–102:221
5. Barzilai S, Aizenshtein M, Froumin N, Frage N (2006) Mater Sci Eng A 420:291
6. Barzilai S, Aizenshtein M, Shapiro-Tsoref E, Froumin N, Frage N (2007) Int J Adhes Adhes 27:358
7. Sobczak N, Nowak R, Radziwiłł W, Stobierski L (2008) In: Sobczak J (ed) Innovation in foundry. Part II (in Polish). Foundry Research Institute, Krakow
8. Fabrichnaya O, Seifert HJ, Ludwig T, Aldinger F, Navrotsky A (2001) Scand J Metall 30:175
9. Sobczak N, Oblakowski J, Nowak R, Kudyba A, Radziwill W (2005) J Mater Sci 40:2313. doi:10.1007/s10853-005-1951-6
10. Sobczak N (2005) Ceram Trans 146:83
11. Sobczak N, Nowak R, Sienicki E, Stobierski L (2010) Arch Metall (to be published)
12. Wojewoda-Budka J, Sobczak N, Morgiel J (2010) J Microsc. doi: 10.1111/j.1365-2818.2009.03237.x
13. Lukas HL, Fries SG, Sundman B (2007) Computational thermodynamics. The Calphad method. Cambridge University Press, Cambridge
14. Rao YK (1985) Stoichiometry and thermodynamics of metallurgical processes. Cambridge University Press, Cambridge
15. Massalski TB, Okamoto H, Subramanian PR, Kacprzak L (1990) Binary alloy phase diagrams. ASM Int, Materials Park
16. Hillert M, Staffanson LI (1970) Acta Chem Scand 24:3618
17. Rapp RA, Ezis A, Yurek GJ (1973) Metall Trans 4:1283
18. SSUB3, SGTE substance database, v 3.2, 2004. Provided by ThermoCalc Software AB